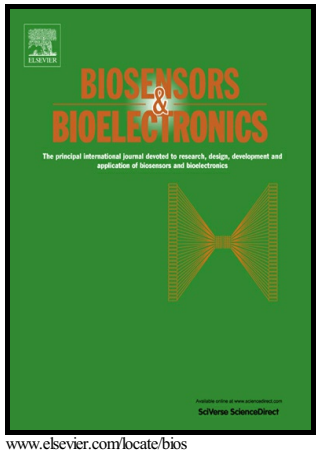

www.elsevier.com/locate/bios

Metal-Enhanced Fluorescence/Visual Bimodal Platform for Multiplexed Ultrasensitive Detection of MicroRNA with Reusable Paper Analytical Devices

Linlin Liang, Feifei Lan, Xuemei Yin, Shenguang Ge, Jinghua Yu, Mei Yan

PII: S0956-5663(17)30275-0
DOI: http://dx.doi.org/10.1016/j.bios.2017.04.027
Reference: BIOS9688

To appear in: *Biosensors and Bioelectronic*

Received date: 26 January 2017
Revised date: 2 April 2017
Accepted date: 20 April 2017

Cite this article as: Linlin Liang, Feifei Lan, Xuemei Yin, Shenguang Ge Jinghua Yu and Mei Yan, Metal-Enhanced Fluorescence/Visual Bimodal Platform for Multiplexed Ultrasensitive Detection of MicroRNA with Reusabl Paper Analytical Devices, *Biosensors and Bioelectronic* http://dx.doi.org/10.1016/j.bios.2017.04.027

Metal-Enhanced Fluorescence/Visual Bimodal Platform for Multiplexed Ultrasensitive Detection of MicroRNA with Reusable Paper Analytical Devices

Linlin Liang[a], Feifei Lan[a], Xuemei Yin[a], Shenguang Ge[a,b*], Jinghua Yu[a], Mei Yan[a]

[a]*School of Chemistry and Chemical Engineering, University of Jinan, Jinan 250022 (P. R. China)*

[b]*Shandong Provincial Key Laboratory of Preparation and Measurement of Building Materials, University of Jinan, Jinan 250022 (P.R. China)*

*Corresponding author. Tel.: +86 531 82767161. E-mail: chm_gesg@163.com

Abstract

Convenient biosensor for simultaneous multi-analyte detection was increasingly required in biological analysis. A novel flower-like silver (FLS)-enhanced fluorescence/visual bimodal platform for the ultrasensitive detection of multiple miRNAs was successfully constructed for the first time based on the principle of multi-channel microfluidic paper-based analytical devices (μPADs). Fluorophore-functionalized DNA_1 (DNA_1-N-CDs) was combined with FLS, which was hybridized with quencher-carrying strand (DNA_2-CeO_2) to form FLS-enhanced fluorescence biosensor. Upon the addition of the target miRNA, the fluorescent intensity of DNA_1-N-CDs within the proximity of the FLS was strengthened. The disengaged DNA/CeO_2 complex could result in color change after joining H_2O_2, leading to real-time visual detection of miRNA firstly. If necessary, then the fluorescence method was applied for a accurate determination. In this strategy, the growth of FLS in μPADs not only reduced the background fluorescence but also provided an enrichment of "hot spots" for surface enhanced fluorescence detection of miRNAs. Results also showed versatility of the FLS in the enhancement of sensitivity and selectivity of the miRNA biosensor. Remarkably, this biosensor could detect as low as 0.03 fM miRNA210 and 0.06 fM miRNA21. Interestingly, the proposed biosensor also possessed good capability of recycling in three cycles upon change of the supplementation of DNA_2-CeO_2 and visual substitutive device. This method opened new opportunities for further studies of miRNA related bioprocesses and will provide a new instrument for simultaneous detection of multiple low-level biomarkers.

Graphical abstract

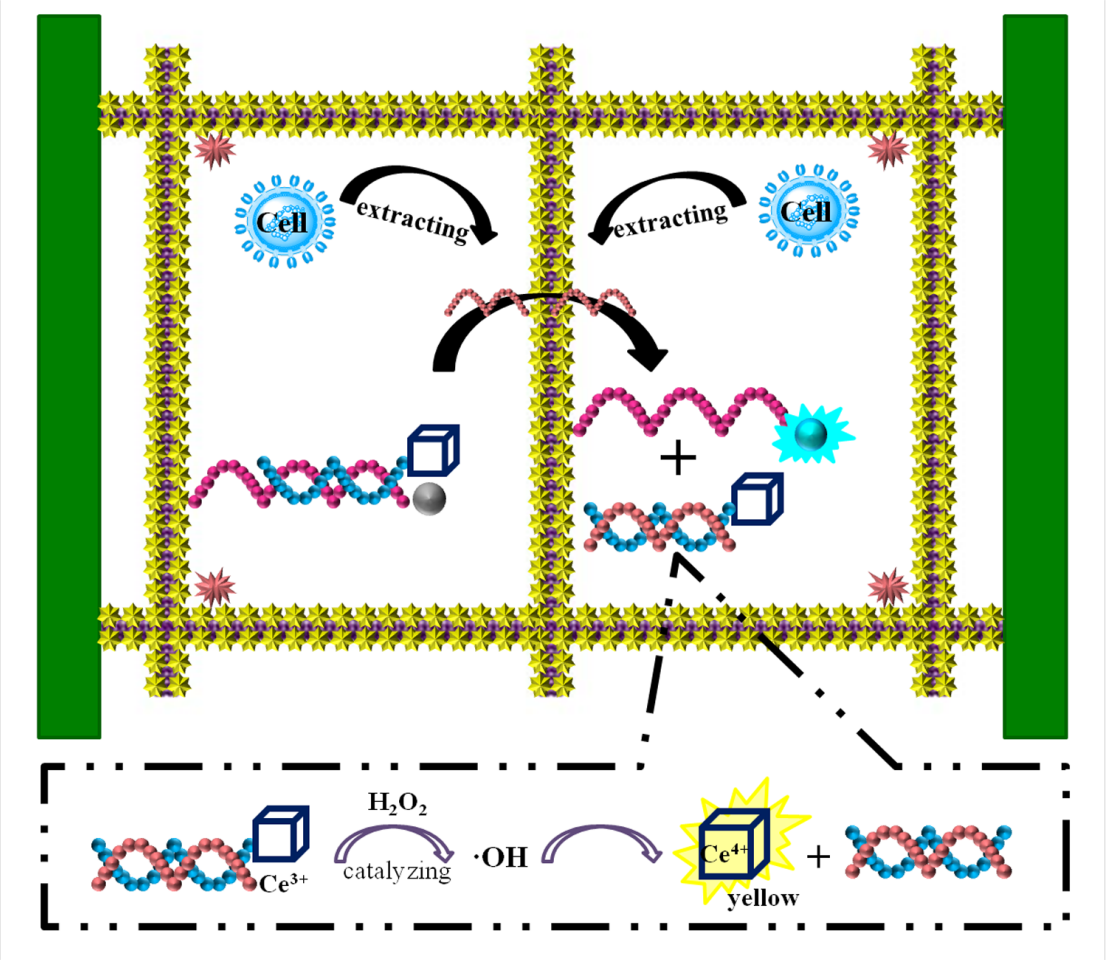

Keywords: FLS-enhanced fluorescence; Visualization; Bimodal platform; Multi-channel μPADs; Recycling

1. Introduction

MicroRNAs (miRNAs) are a class of single-stranded, endogenous, nonprotein-coding RNAs (approximately 18-25 nucleotides), which have essential functions in almost every normal and pathologic processes (Jing et al., 2015; Yang et al., 2012; Ventura et al., 2009; Cissell et al., 2007; Lu et al., 2005). The growing evidence testified that their expression level of miRNAs is closely associated with some major human diseases (Keller et al., 2011; Ryan et al., 2010). Hence, quantitative measurements of miRNAs expression were crucial to early diagnosis, diseases cure. And they may significantly improve disease diagnosis in reducing the

proportion of false positives or substituting uncomfortable traditional diagnosis methods (Jou et al., 2015; Tran et al., 2014). Nevertheless, analysis of miRNAs in clinical samples remains a great challenge on account of sequence similarity among family members, their short sequences and especially low abundance (Lee et al., 2008). Currently, many newly developed methods have been employed for miRNA analysis, including microarrays, electrocatalysis, miRNA array technology and real-time quantitative polymerase chain reaction. They often suffer from problems such as time-consuming operation, low sensitivity, significant false positives and enzyme engagement, etc (Jin et al., 2015; Degliangeli et al., 2014; Dodgson et al., 2012; Zhou et al., 2015).

Microfluidic paper-based analytical devices (μPADs) have attracted increasing interest in cytological tests or histological for implementing in situ, visual, simple, miniaturized testing since Martinez and co-workers initiated this domain from 2007 (Martinez et al., 2007). To date, various visual μPADs about analytical methods have primarily utilized for the qualitative detection of polytype analytes on account of their simplicity, naked eye and low-cost (Li et al., 2016; Zhang et al., 2017; Ge et al., 2017). However, there was a strong need to solve the problem of the low sensitivity. The fluorescence methods been paid attention to widely because of their fast response time, high sensitivity and the ability to provide in situ and real-time information (Zhu et al., 2016; Yuan et al., 2012). Nanoceria (CeO_2) has received a great deal of research interest due to its regeneration or autocatalysis (Laberty et al., 2007). Upon addition of H_2O_2, the color of CeO_2 changes from colorless to orange in a concentration-dependent manner. More importantly, CeO_2 strongly adsorbed DNA and was a remarkable fluorescence quencher (Xu et al., 2014; Pautler et al., 2013). Herein, we firstly structured a microfluidic paper-based fluorescence/visual bimodal platform, which combined the merits of the visual detection for screening and fluorescence detection for quantitative analysis. It could effectively make the detection more convincing.

Nevertheless, owing to grievous background fluorescence of additives and scattering light in the paper substrate, it is very hard to realize fluorescence detection

directly on μPAD (Nery et al., 2013). To meet the challenge, an interconnected dense flower-like silver (FLS) layer was grown on the surfaces of cellulose fibers in the fluorescence detection zone, which could effectively reduce the paper background fluorescence signal. Moreover, the active surface area and the sensitivity of this FLS-μPAD was much higher than that of a bare one. Interestingly, the fluorescence resonance energy transfer efficiency (FRET) could be dramatically enhanced through silver-fluorophore interaction and utilizing the phenomenon named metal-enhanced fluorescence (MEF), which giving rise to an augment in the emission intensity of nearby fluorophores (Lukomska et al., 2004; Zhang et al., 2007; Liang et al., 2017; Lessard et al., 2009). The MEF effect was closely related with shape and species of nanoparticles as well as distance between silver and fluorophores (Zhang et al., 2008; Chen et al., 2007; Wang et al., 2012). Thus, the phenomenon of silver-enhanced FRET efficiency has been reported. Currently, a variety of biosensors have been attracting increasing interest for the multiplexed detection of miRNA. Compared with single-marker detection, multiplexed detection possessed the merits of lowered detection cost, shortened analytical time and improved detection throughput (Barbee et al., 2010; Lai et al., 2011). Therefore, in our work, we have achieved multiplexed detection of miRNAs through projecting multi-channel μPADs and different recognition probes.

Inspired by previous study, in our manuscript, we fabricated a simple and novel FLS-enhanced fluorescence/visual bimodal biosensor for multiplexed detection of miRNA with low fluorescence background and high sensitivity based on multiplexed μPADs. As a model, two biomarkers, miR210 and miR21, displaying enormous significance in some cancer screening and early clinical diagnosis of the diseases, were used as model bioanalytes. Compared with the previously reported detection constructions, our proposed biosensor possessed some significant advantages: (1) FLS-μPADs could not only effectively reduce the paper background fluorescence but also greatly improve the detection sensitivity by silver-enhanced FRET efficiency. (2) In our work, CeO_2 not only serve as a nanozyme with oxidase activity because of its regeneration or autocatalysis but also was an excellent fluorescence quencher. (3) The

multiplexed detection of miRNA was realized by design of multi-channel μPADs, and the FLS-μPADs were recycled upon change of visual substitutive device and supplementation of DNA_2-CeO_2. (4) The proposed biosensor combined FLS-enhanced fluorescence/visual bimodal platform to naked-eye detection of miRNA. As a consequence, the developed miRNA biosensor holds potential for ultrasensitive, multiplexed and visual detection of miRNA and it could be extended to other assay formats for various analytes of interest in our future work.

2. Experimental

2.1. Fabrication of reusable μPADs

The reusable μPADs were prepared by our previously reported method with large modifications for fluorescence/visual bimodal detection of miRNA (Ge et al., 2012; Zhang et al., 2014). As shown in Scheme 1A, the reusable μPADs were fabricated through wax-printing, which were comprised of one detection tab and two channel tabs with the same size (40.0 mm×40.0 mm). On the detection tab, the hydrophilic area in white with the diameter of 4 mm was sampling zone. The four white areas with diameter of 6 mm locating similarly to Zone a were used for fluorescence detection and the other four hydrophilic areas like Zone b on the edge of the tab were for visual detection. On the Channel tab 1, the circle areas are punching zones and the rectangular channels (3 mm length × 2 mm width) were hydrophilic areas connecting the sampling zone and three of the fluorescence detection zones for the flow of miRNA samples depending to the capillary action of paper. The only fluorescence zone without linking channel was used as a blank control. The channels of the same size on Channel tab 2 were used for the flow of residues from fluorescence detection zones to visual ones. According to the design, we prepared origami the device in Scheme 1B. Along fold line I, the sampling zone and fluorescence detection zone would be connected to form fluorescence detection device (the upper part in Scheme 1C). For visual detection, the visual substitutive tab (Scheme 1D) was placed on the fluorescence detection device and Channel tab 2 was folded over them. Taking

advantages of the paper's capillary effects, the visual tab could receive the fluid from fluorescence zone for visual detection of miRNA (Scheme 1E). Meanwhile, the fluorescence device recovered to the original state, which thus could be reusable. The detailed fabrication procedures were described in Supporting Information (SI, Fig. S1-S4) and the corresponding detection mechanism was shown in Scheme 2.

2.2. Fabrication of FLS-μPADs

Prior to the immobilization, so as to decrease backgroud, magnify signal and enlarge effective surface area for sensitive immunosensing, the novel FLS layer was growed on the surfaces of cellulose fibers in the fluorescence detection zone of μPADs (Jana et al., 2001). And a detailed procedure was described in the supplementary information.

2.3. Preparation of DNA_1-N-CDs

Nitrogen-doped carbon nanodot (N-CDs) were prepared by a single-mode microwave synthesizer (Tang et al., 2014). And detailed procedures of N-CDs and DNA_1-N-CDs were described in the supplementary information.

2.4. Preparation of DNA_2-CeO_2

Preparation of DNA_2-CeO_2: The typical synthesis procedure of CeO_2 (Xie et al., 2015) was described in the supplementary information. And preparation of DNA_2-CeO_2 was described as follows. Firstly, the CeO_2 surface was silylated with APTES. Then, amino-functionalized CeO_2 were dispersed in a mixture of 200 μL of DNA_2 (10 μM), 100 μL EDC (20 mg mL^{-1}) and 50 μL NHS (20 mg mL^{-1}). And the mixture was stirred for 12 h. The DNA_2-CeO_2 was collected by centrifugation and extensively washed with water.

2.5. Operation and assay procedures of this biosensor

The fabrication and the assay procedure of this microRNA biosensor were shown in Scheme 2, and a detailed procedure was described below. Briefly, on the detection

tab a, 10 μL of DNA_1-N-CDs was dropped into FLS-μPADs, and incubated at room temperature for 1 h. Physically absorbed excess DNA_1-N-CDs was removed by careful and thorough rinsing. After that, The nonspecific binding sites were blocked by injecting 10 μL 2% BSA into the detection tab a, which was incubated for 5 min at room temperature. Subsequently, 10 μL of DNA_2-CeO_2 was added to paper cell zones to act as an efficient fluorescence quencher. The superfluous DNA_2-CeO_2 were carefully and thoroughly washing with PBS. After folding along line Ⅰ, the channel tab1 was placed over the detection tab (Scheme 1C), 60 μL of microRNA (which was extracted from cancer cells using the MirVana microRNA isolation kit according to the manufacturer's procedures) was dropped into the middle area and incubated at room temperature for 15 min. Then, the fluorescent spectra were measured using a FLS920 Edinburgh Fluorescence Spectrometer under excitation at 390 nm. Based on the fluorescence device, visual detection zone was constructed according to Scheme 1E. Then 20 μL of 5 mM H_2O_2 were added to the each of visual detection zones and incubated for 15 min. A fast color change occurred, which could be easily distinguished by naked eyes.

3. Results and discussion

3.1. Characterization of the modified papers

FLS-μPADs not only increased the surface areas and effectively reduced the background fluorescence of paper fibers but also magnified signal due to the MEF effect of AgNPs. The novel FLS-μPADs were fabricated via a seed-mediated synthetic method by using $AgNO_3$ as metal sources and AA as a reductant. The morphologies of the FLS-μPADs were characterized by SEM. The porous bare cellulose paper with smooth microfibers (Fig. 1A), possessed high ratio of surface area to weight (9.5 m^2/g) (Pelton et al., 2009), which could provide an excellent adsorption microenvironment for AgNP seeds. After 10 min of growth, a continuous and dense FLS layer on the cellulose fiber surfaces in fluorescence detection zone was observed in Fig. 1B and C.

The prepared FLS-μPADs still keeped good porous structure, which would help further modification and research. In addition, XRD analysis was performed to confirm the crystal structures of FLS-μPADs and bare μPADs (Fig. 1D). Curve a showed that one representative diffraction reflection at 14.2°, 14.8°, 22.8°, which was matched well with the cellulose (002) plane (JCPDS 03-0289). In contrast to the XRD of bare μPADs, FLS-μPADs showed four reflections at 38.2°, 44.4°, 64.6° and 77.5° (curve b), which may be indexed to the (111), (200), (220) and (311) facets of silver respectively, clearly declaring the successful preparation of FLS-μPADs.

3.2. Characterization of N-CDs and CeO_2

The N-CDs were obtained by a microwave-assisted onepot solvothermal growth method. The TEM images (Fig. 2A) indicated that most of the N-CDs were uniform and well dispersed with diameters in the range of 4-7 nm. Under the excitation of 365 nm UV light, the N-CDs possessed bright blue color (inset) and stable photostability with a transparent appearance. The fluorescence spectra of the N-CDs showed the excitation dependent emission (Fig. 2B), which exhibited the maximum excitation wavelength at 390 nm and a sharp peak centered at 462 nm. The fluorescence quantum yield of the N-CDs were 41%, much higher than that of undoped CDs (35%), which was ascribed to the nitrogen doping undoubtedly. The surface composition and elemental analysis for the N-CDs were investigated by X-ray photoelectron spectra (XPS). The full range XPS analysis (inset in Fig. 2C) of the N-CDs showed three typical peaks at 284.1, 400.1, and 496.1 eV, which were ascribed to C 1s, N 1s, and O 1s, respectively. The high-resolved spectrum of C1s (Fig. 2C) could be deconvoluted into four single peaks that correspond to C-C (sp3, 284.5 eV), C-N (sp3, 286.1 eV), C-O (sp2, 287.9 eV), and C=O (sp2, 288.7 eV) bonds. This indicated that the surfaces of N-CDs were rich in hydrophilic groups on the surfaces, which were in good agreement with the FT-IR results (Fig. S5).

The morphologies of the CeO_2 were observed by SEM and TEM. SEM

observation of the CeO_2 (Fig. 2D) suggested that the products had a good dispersibility and a narrow distribution of diameters in the range of 13-15 nm. Similar results were obtained by the corresponding TEM characterization (Fig. 2E). X-ray diffraction (XRD) patterns of the as-prepared CeO_2 were shown in Fig. 2F. The peaks at 2θ values of 28.6, 33.1, 47.5, 56.4, 59.3, 69.3, 76.8 and 79.0 can be indexed to (111), (200), (220), (311), (222), (400), (331) and (420) crystal planes, respectively. All the diffraction peaks can be directly indexed to a pure phase of face-centered cubic ceria structures (JCPDS 34-0394), which are consistent with the corresponding TEM or SEM.

3.3 Possible Mechanism for this Biosensor

The miRNA fluorescence biosensor was fabricated based on the recovery of the quenched fluorescence of DNA_1-N-CDs that was tightly bound to the DNA_2-CeO_2. The mechanism of this metal-enhanced fluorescence biosensor was shown in Scheme 1A. The as-prepared nanoassembly was found to give very weak fluorescence after quenching by DNA_2-CeO_2, indicating very high fluorescence quenching efficiency for N-CDs by CeO_2. By contrast, incubation of the nanoassembly with miRNA resulted in a recovery of the fluorescence signal. At this moment, N-CDs were close to the FLS to enhance their fluorescence by MEF effect (Fig. S8 and Fig. S7). Thus, the detection sensitivity could be increased largely. The fluorescence device recovered to the original state, which thus could be reusable by supplementing DNA_2-CeO_2. In addition, as illustrated in Scheme 2B, free DNA_2-CeO_2 released from target miRNA was used to perform visual monitoring. After adding H_2O_2, it is generally accepted that the color change was due to oxidation of Ce^{3+} to Ce^{4+} (Sardesai et al., 2013; Das et al., 2007).

3.4. Sensitivity and feasibility of the FLS-Enhanced FRET Sensor

In order to validate the sensitivity and feasibility of the proposed biosensor in multiplexed ultrasensitive detection for miRNA, the synthetic miRNA21 and

miRNA210 sequences were chosen as miRNA targets (supporting information). After the optimization of experimental conditions (Fig. S8), 10 μL CeO_2 was used for this research and the fluorescent pictures from sensor detection could be clearly monitored by naked eye under the UV lamp. From Fig. 3, the fluorescence intensity and color change with different concentrations of miRNA were measured to evaluate the sensitivity and the quantitative range of the proposed biosensor. The relationship between fluorescence intensity and concentrations of miRNA (miRNA210 and miRNA21) was shown in Fig. 3. Fluorescence signal increased gradually with the increasing concentration of miRNA. As shown in Fig. 3B,C and Fig. 3E,F, a good linear relationship of fluorescence intensity and the concentrations of miRNA was achieved in the range from 0.1 fM to 1 nM and 0.2 fM to 2 nM for miRNA210 and miRNA21, respectively. The linear regression equations for miRNA210 and miRNA21 could be represented as $\Delta F = 126.80 + 96.48 \lg c_{\mathrm{miRNA210}}$ with the correlation coefficient of R = 0.9987, $\Delta F = 103.15 + 91.79 \lg c_{\mathrm{miRNA21}}$ with the correlation coefficient of R = 0.9966, respectively. Moreover, their detection limits (three times the standard deviation above the blank, n = 6) were estimated to be 0.03 and 0.06 fM, respectively. The proposed novel biosensor showed a better performance compared to other reported methods (Table 1), especially the detection limit. In addition, free DNA_2-CeO_2 released from target miRNA was used to execute visual detection of miRNA. The color turned from colorless to yellow and gradually deepened with increasing concentrations of miRNA and the change of color could be readily observed by the naked eyes. The gray scale analysis revealed a good linear relationship between the gray intensity and the concentrations of miRNA (Fig. 3A,D). The results indicated that the proposed biosensor possessed higher sensitivity and could be suitable for the practical visual detection of miRNA in real sample.

3.5. Recyclability, stability, specificity and reproducibility of the biosensor

It was a remarkable fact that the most of current μPADs could not be cyclically used (Li et al., 2016; Ge et al., 2012). Therefore, it was strongly hoped to establish a

recyclable μPADs. In our work, after the first round reaction, which was rinsed with 0.1 M PBS buffer solution (pH 7.4) thoroughly. Upon supplementation of DNA_2-CeO_2, the dsDNA structure was regenerated by the rehybridization between DNA_1-N-CDs and DNA_2-CeO_2, and then upon change of visual substitutive device, the FLS-μPADs was regenerated and used for the next cycle detection. The detection results were revealed in Fig. 4A. It displayed that the FLS-μPADs could be repeated at least three times without significant change of the fluorescence intensity, manifesting the good recyclability of this FLS-μPADs.

A key factor of the proposed biosensor was the stability in their application and development. So, the five as-prepared FLS-μPADs were stored at 4 ºC. At different storage times (0, 1, 2, 3 and 4 weeks), one of these FLS-μPADs was taken out for measurement. As can be seen in Fig. 4B, after a week of storage, the signal intensity did not show any significant changes. In addition, the storage time was extended to 4 weeks, the proposed biosensor reserved about 91.4% of its original response. The result indicated that the proposed biosensor had acceptable storage stability.

The specificity of the proposed biosensor was investigated in solution by using four different miRNA sequences, including without miRNA, the miRNA21, miRNA210, miRNA141, let-7a, let-7c and mixture of forenamed miRNA with the same concentration. As depicted in Fig. 4C, compared to the blank test (without miRNA), the fluorescence intensity for the presence of the control sequences (miRNA141, let-7a, let-7c) showed negligible changes. And the mixture in the presence of target miRNA has negligibly influence on the fluorescence intensity of target miRNA. These above results demonstrated that the proposed biosensor had high selectivity toward target miRNA against other control sequences.

The reproducibility of the proposed biosensor was crucial requirements for any practical applications, which was explored by intra- and inter-assay relative standard deviation (RSD). The proposed biosensor prepared on the same and different batches were used to test the two different miRNA with the same concentration, respectively. These results demonstrated that their RSDs of five parallel determinations were less

than 3% for the same batch biosensor, and less than 4% for different batch biosensor, indicating that the reproducibility of the proposed method was acceptable.

3.6. Detection of clinical samples

The clinical diagnosis of the proposed biosensor was researched by detecting miRNA210 in three different cell lysates: MCF-7 (breast adenocarcinoma cells), A549 (lung adenocarcinoma cells) and HepG2 (hepatocellular liver carcinoma cells). All the clinical tumor tissues were pretreated with liquid nitrogen and ground into a paste, followed by total miRNA extraction by a MirVana microRNA isolation kit. In this test, 30 clinical tumor samples were detected, each group isolated from 1 g of tumor tissue. The results were observed and recorded in Fig. 4D-F. Also, 23 of 30 tumor samples contained the miR-210 levels exceeding their estimated reference intervals. Hence, this miRNAs detection platform possesses potentials to be a versatile strategy for tumor molecular diagnosis technologies. Considering the tumor tissues and normal tissues are intertwined, the researchers could get a high precision by increasing sample dose and multidraw of tumor tissue. In addition, the standard addition method, using synthetic miRNA210 as the standard, respectively, was used to measure the concentration of miRNA210 in MCF-7 cells. Subsequently, 200 μL of MCF-7 cells spiked with different concentrations of miRNA210 was dropped onto the proposed biosensor. The results of MCF-7 cells were shown in Table S1, the recovery values ranged from 96.88-103.0%. The obtained results were with consistence to the traditional real-time polymerase chain reaction (RT-PCR), which indicated that the proposed biosensor had potentiality in examination of miRNA210 in real biological samples.

4. Conclusions

In conclusion, we have demonstrated a novel metal-enhanced fluorescence/visual bimodal platform for the multiplexed detection of miRNAs by designing μPADs and different fluorescence probes. Without the target miRNAs, the formation of double-stranded DNA shorten the spacing distance between the N-CDs and the CeO_2,

which significantly quenching the fluorescence of N-CDs. While in the presence of target miRNAs, the fluorescence of quenched probe was recovered, leading to an in situ quantitative method. Firstly, preliminary detection of miRNAs was performed by naked eye. The disengaged DNA/CeO_2 complex could result in color change after adding H_2O_2 because of autocatalysis of CeO_2, resulting in real-time visual detection of miRNAs. If further accurate determination was required, fluorescence detection was applied. FLS-μPADs provided an enrichment of "hot spots" for surface enhanced fluorescence detection of miRNAs and were significant for the final enhancement of detection sensitivity. In addition, the proposed biosensor also possessed good capability of recycling in three cycles by means of the supplementation of DNA_2-CeO_2 and visual substitutive device. More importantly, our methods have been challenged in real samples and achieved satisfactory result. With reliance on the instinctive properties proposed above, the principle of this assay could be extended to other proteins or new biomarkers for disease diagnosis and fundamental research.

Acknowledgements

This work was financially supported by National Natural Science Foundation of China (21575051, 21475052, 51502112), National High-tech R & D Program (863 Program, 2015AA034701), and Key Research and Development Program of Shandong Province, China (2016GGX102035).

References

Barbee, K.D., Hsiao, A.P., Roller, E.E., Huang, X.H., 2010. Lab. Chip. 10, 3084-3093.

Causa, F., Aliberti, A., Cusano, A.M., Battista, E., Netti, P.A., 2015. J. Am. Chem. Soc. 137, 1758-1761.

Chen, Y., Munechika, K., Ginger, D.S., 2007. Nano Lett. 7, 690-696.

Cissell, K.A., Shrestha, S., Deo, S.K., 2007. Anal. Chem. 79, 4754-4761.

Das, M., Patil, S., Bhargava, N., Kang, J.F., Riedel, L.M., Seal, S., Hickman, J.J., 2007. Biomaterials 28, 1918-1925.

Degliangeli, F., Kshirsagar, P., Brunetti, V., Pompa, P.P., Fiammengo, R., 2014. J. Am.

Chem. Soc. 136, 2264-2267.

Dodgson, B.J., Mazouchi, A., Wegman, D.W., Gradinaru, C.C., Krylov, S.N., 2012. Anal. Chem. 84, 5470-5474.

Ge, L., Yan, J.X., Song, X.R., Yan, M., Ge, S.G., Yu, J.H., 2012. Biomaterials 33, 1024-1031.

Ge, S.G.; Zhang, L.N.; Zhang, Y.; Lan, F.F.; Yan, M.; Yu, J.H., 2017. Nanoscale 9, 4366-4382

Ge, Z.L., Lin, M.H., Wang, P., Pei, H., Yan, J., Shi, J.Y., Huang, Q., He, D.N., Fan, C.H., Zuo, X.L., 2014. Anal. Chem. 86, 2124-2130.

Jana, N.R., Gearheart, L., Murphy, C.J., 2001. Chem. Commun. 617-618.

Jing, Z., Han, W.D., Sui, X.B., Xie, J.S., Pan, H.M., 2015. Cancer Lett 356, 332-338.

Jin, Z., Geiβler, D., Qiu, X., Wegner, K.D., Hildebrandt, N., 2015. Angew. Chem., Int. Ed. 54, 10024-10029.

Jou, A.F.J., Lu, C.H., Ou, Y.C., Wang, S.S., Hsu, S.L., Willner, I., Ho, J.A.A., 2015. Chem. Sci. 6, 659-665.

Keller, A., Leidinger, P., Bauer, A., Elsharawy, A., Haas, J., Backes, C., Wendschlag, A., Giese, N., Tjaden, C., Ott, K., 2011. Nat. Methods 8, 841-843.

Laberty-Robert, C., Long, J.W., Pettigrew, K.A., Stroud, R.M., Rolison, D.R., 2007. Adv. Mater. 19, 1734-1739.

Lai, G.S., Wu, J., Ju, H.X., Yan, F., 2011. Adv. Funct. Mater. 21, 2938-2943.

Lee, I., Ajay, S.S., Chen, H., Maruyama, A., Wang, N., McInnis, M.G., Athey, B.D., 2008. Nucleic Acids Res. 36, e27.

Lessard-Viger, M., Rioux, M., Rainville, L., Boudreau, D., 2009. Nano Lett. 9, 3066-3071.

Liang, L.L., Lan, F.F., Ge, S.G., Yu, J.H., Ren, N., Yan, M., 2017. Anal. Chem. 89, 3597-3605

Li, L., Zhang, Y., Zhang, L.N., Ge, S.G., Liu, H.Y., Ren, N., Yan, M., Yu, J.H., 2016. Anal. Chem. 88, 5369-5377.

Lukomska, J., Malicka, J., Gryczynski, I., Lakowicz, J.R., 2004. J. Fluoresc. 14, 417-423.

Lu, J., Getz, G., Miska, E.A., Alvarez-Saavedra, E., Lamb, J., Peck, D., Sweet-Cordero, A., Ebert, B.L., Mak, R.H., Ferrando, A.A., Downing, J.R., Jacks, T., Horvitz, H.R., Golub, T.R., 2005. Nature 435, 834-838.

Martinez, A.W., Phillips, S.T., Butte, M.J., Whitesides, G.M., 2007. Angew. Chem., Int. Ed. 46, 1318-1320.

Miao, P., Wang, B.D., Chen, X.F., Li, X.X., Tang, Y.G., 2015. ACS Appl. Mater. Interfaces 7, 6238-6243.

Nery, E.W., Kubota, L.T., 2013. Anal. Bioanal. Chem. 405, 7573-7595.

Pautler, R., Kelly, E.Y., Huang, P.J.J., Cao, J., Liu, B., Liu, J., 2013. ACS Appl. Mater. Interfaces 5, 6820-6825.

Pelton, R., 2009. Trends in Anal. Chem. 28, 925-942.

Ryan, B.M., Robles, A.I., Harris, C.C., 2010. Nat. Rev. Cancer 10, 389-402.

Sardesai, N.P., Andreescu, D., Andreescu, S., 2013. J. Am. Chem. Soc. 135, 16770-16773.

Tang, J., Zhang, Y.Y., Kong, B., Wang, Y.C., Da, P.M., Li, J., Elzatahry, A.A., Zhao, D.Y., Gong, X.G., Zheng, G.F., 2014. Nano Lett. 14, 2702-2708.

Tran, H.V., Piro, B., Reisberg, S., Nguyen, L.H., Nguyen, T.D., Duc, H.T., Pham, M.C., 2014. Biosens. Bioelectron. 62, 25-30.

Ventura, A., Jacks, T., 2009. Cell 136, 586-591.

Wang, Y., Li, Z., Li, H., Vuki, M., Xu, D., Chen, H.Y., 2012. Biosens. Bioelectron. 32, 76-81.

Xie, A.R., Wang, S.P., Liu, W., Zhang, J.C., Yang, Y.Z., Han, J.T., 2015. Materials Research Bulletin 62,148-152.

Xu, C., Liu, Z., Wu, L., Ren, J., Qu, X., 2014. Adv. Funct. Mater. 24, 1624-1630.

Xu, F.F., Yang, T., Chen, Y., 2016. Anal. Chem. 88, 754-763.

Yang, L., Liu, C.H., Ren, W., Li, Z.P., 2012. ACS Appl. Mater. Interfaces 4, 6450-6453.

Yuan, C., Zhang, K., Zhang, Z., Wang, S., 2012. Anal. Chem. 84, 9792-9801.

Zhang, J., Fu, Y., Chowdhury, M.H., Lakowicz, J.R., 2008. J. Phys. Chem. C 112, 18-26.

Zhang, Y., Ge, L., Li, M., Yan, M., Ge, S.G., Yu, J.H., Song, X.R., Cao, B.Q., 2014. Chem. Commun. 50, 1417-1419.

Zhang, Y., Li, L., Zhang, L.N., Ge, S.G., Yan, M., Yu, J.H., 2017. Nano Energy 31, 174-182.

Zhang, J., Fu, Y., Lakowicz, J.R., 2007. J. Phys. Chem. C 111, 50-56.

Zhou, X., Cao, P., Zhu, Y., Lu, W., Gu, N., Mao, C., 2015. Nat. Mater. 14, 1058-1064.

Zhu, Y., Hu, X.C., Shi, S., Gao, R.R., Huang, H.L., Zhu, Y.Y., Lv, X.Y., Yao, T.M., 2016. Biosens. Bioelectron. 79, 205-212.

Scheme 1 The schematic representation, size, and shape of the HC-μPADs. Paper sheets were firstly patterned in bulk using a wax printer. After laser cut and modification, the device was used to detect miRNA released from tumor cells.

Scheme 2 Schematic representation of the fabrication procedures for the fluorescence detection zone and fluorescence detection mechanism (A) and visual detection mechanism (B) of miRNA released from A549 cells.

Fig. 1. SEM images of (A) pure paper fibers, (B,C) Enlarged FLS layer in paper working zone under different magnification; (D) XRD patterns of the bare μPADs (a); FLS-μPADs (b).

Fig. 2. (A) TEM images of N-CDs. (B) Fluorescence spectra of the N-CDs. The fluorescence spectra were recorded from 320 to 420 nm. (C) High-resolution XPS spectra of the C1s (inset: XPS spectra). (D) SEM image, (E) TEM images, and (F) XRD pattern of the typical CeO_2 nanoparticles.

Fig. 3. visual response of miRNA210 [10 fM, 100 fM, 1 pM, 10 pM, 100 pM, 1 nM (a-f)] (A) and miRNA21 [20 fM, 200 fM, 1 pM, 10 pM, 100 pM, 2 nM (a-f)] (D) at the concentrations of 10 fM, 100 fM, 1 pM, 10 pM, 100 pM, 1 nM (a-f); Inset: photo of the above samples. fluorescence responses of this biosensor towards different concentrations of miRNA210 (B,C) and miRNA21 (E,F) from 0.1 fM to 1 nM and 0.2 fM to 2 nM in pH 7.4 PBS buffer.

Fig. 4. (A) the fluorescence intensity when the FLS-μPADs is recycling for three times. (B) The storage stability of the proposed biosensor for the miRNA in a refrigerator (4 ˚C). (C) Selectivity investigation of the proposed method for (a) without miRNA, (b) miRNA21, (c) miRNA210, (d) miRNA141, (e) let-7a, (f) let-7c, (g) mixture of forenamed miRNA with the same concentration (100 pM miRNA210 as a model). Tests of tumor tissues with the proposed detection platform: (D) tests of breast adenocarcinoma tissues, (E) tests of lung adenocarcinoma tissues, (F) tests of hepatocellular liver carcinoma tissues.

Table 1. The comparison for different miRNA detection methods

Method	Linear range	Detection limit	References
Fluorescence	1 fM to 1 nM	1 fM	(Causa et al., 2015)
LC-MS/MS	1 pM to 100 nM	1 pM	(Xu et al., 2016)

Electrochemical	1 fM to 100 pM	100 aM	(Ge et al., 2014)
Fluorescence	1 fM to 1 nM	0.4 fM	(Miao et al., 2015)
Fluorescence	miR210: 0.1 fM to 1 nm; miR21: 0.2 fM to 2 nm	miR210: 0.03 miR21: 0.06 fM	This work

LC-MS/MS: Liquid chromatography-tandem mass spectrometry

Highlights

- The proposed biosensor combined FLS-enhanced fluorescence and visual bimodal methods.
- FLS-μPADs could reduce the paper background fluorescence and improve sensitivity by silver-enhanced FRET efficiency.
- The multiplexed detection of miRNA was realized by design of multi-channel μPADs,
- the FLS-μPADs were recycled upon change of visual substitutive device and supplementation of DNA_2-CeO_2.

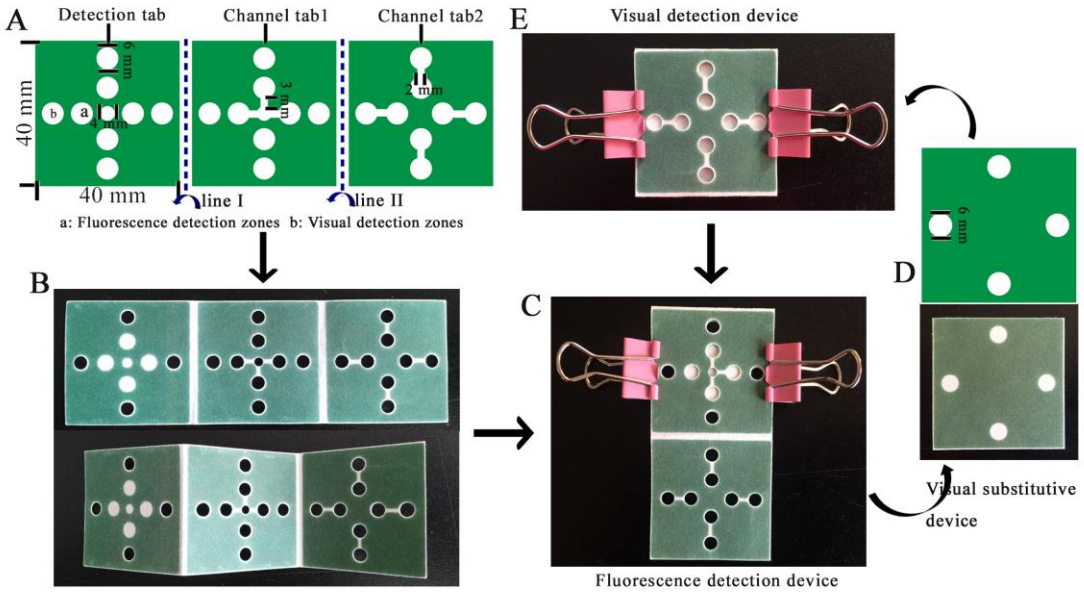
A
Detection tab
Channel tab1
Channel tab2
40 mm
6 mm
3 mm
2 mm
4 mm
40 mm
line I
line II
a: Fluorescence detection zones b: Visual detection zones
B
C
E
Visual detection device
D
6 mm
Visual substitutive device
Fluorescence detection device

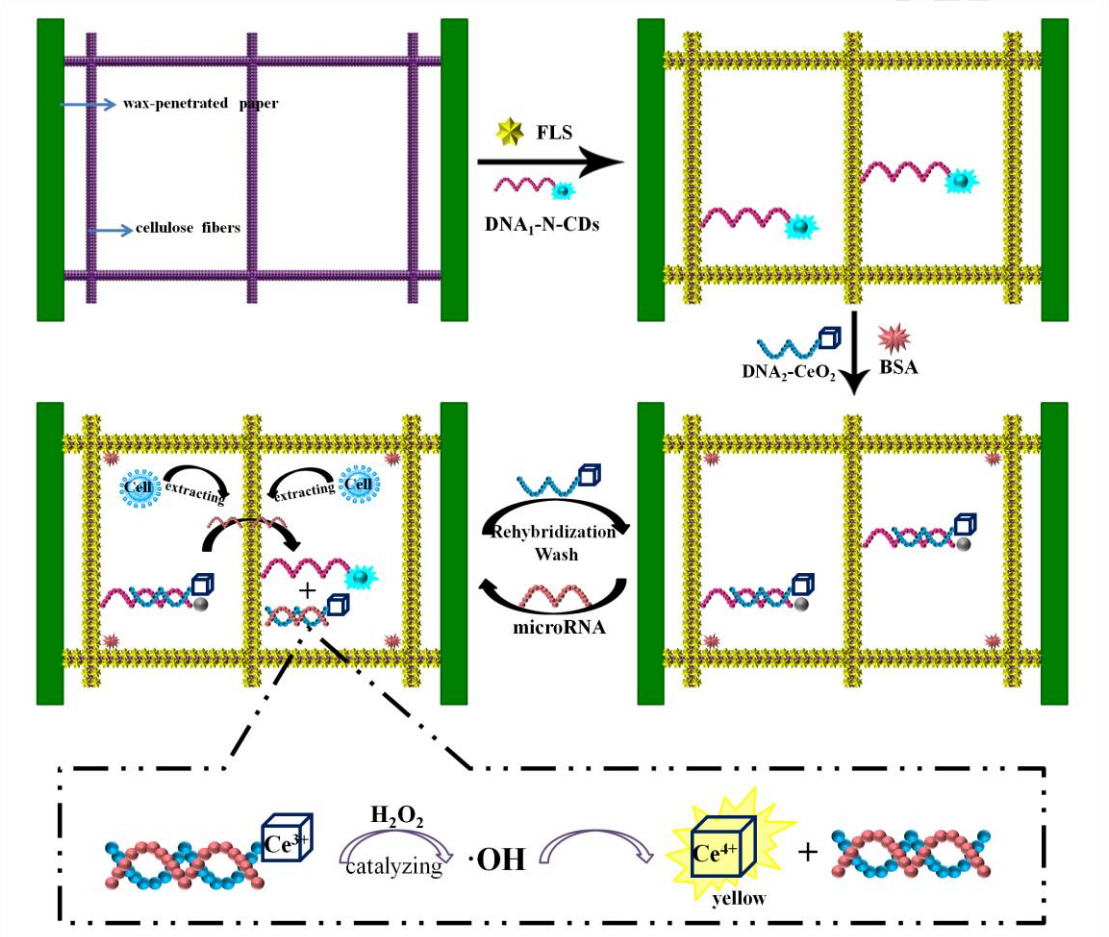
wax-penetrated paper
cellulose fibers
FLS
DNA1-N-CDs
DNA2-CeO2
BSA
Cell
extracting
Rehybridization
Wash
microRNA
H2O2
catalyzing
·OH
Ce3+
Ce4+
yellow

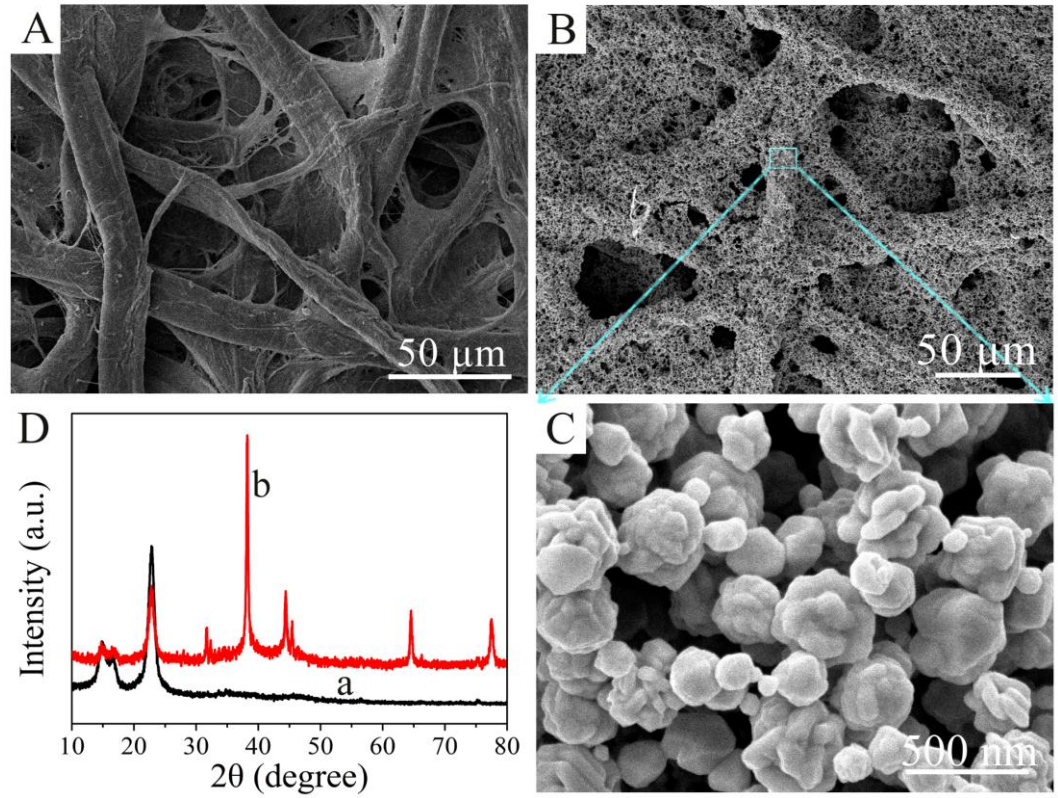
A
50 μm
B
50 μm
D
Intensity (a.u.)
b
a
10 20 30 40 50 60 70 80
2θ (degree)
C
500 nm

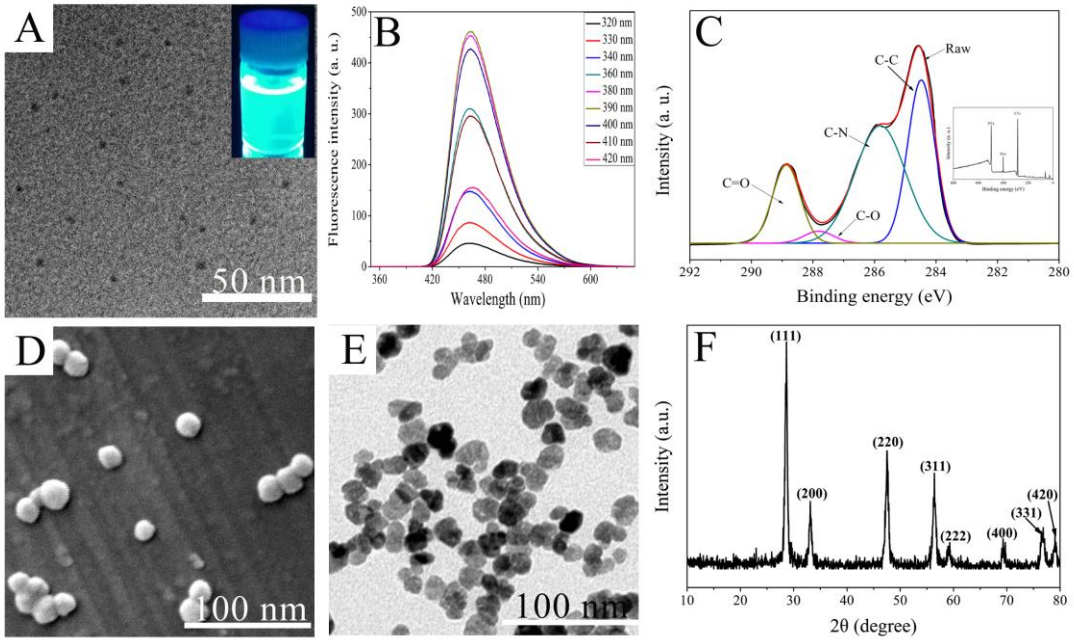
A
50 nm
B
Fluorescence intensity (a. u.)
320 nm
330 nm
340 nm
360 nm
380 nm
390 nm
400 nm
410 nm
420 nm
360 420 480 540 600
Wavelength (nm)
C
Raw
C-C
C-N
C=O
C-O
Intensity (a. u.)
292 290 288 286 284 282 280
Binding energy (eV)
D
100 nm
E
100 nm
F
Intensity (a.u.)
(111)
(200)
(220)
(311)
(222)
(400)
(331)
(420)
10 20 30 40 50 60 70 80
2θ (degree)

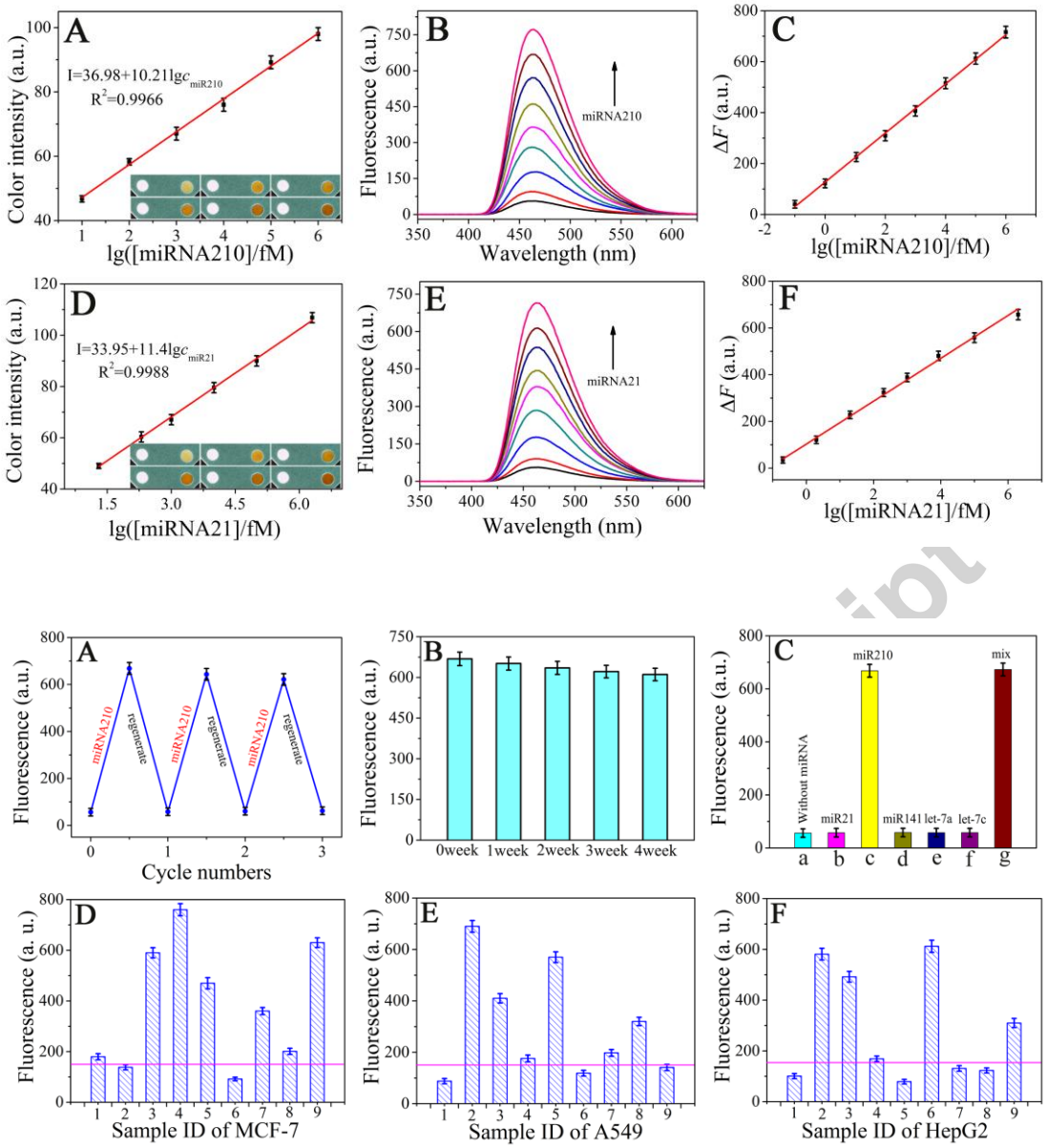
A
I=36.98+10.21lgc miR210
R2=0.9966
Color intensity (a.u.)
lg([miRNA210]/fM)
B
miRNA210
Fluorescence (a.u.)
Wavelength (nm)
C
ΔF (a.u.)
lg([miRNA210]/fM)
D
I=33.95+11.4lgc miR21
R2=0.9988
Color intensity (a.u.)
lg([miRNA21]/fM)
E
miRNA21
Fluorescence (a.u.)
Wavelength (nm)
F
ΔF (a.u.)
lg([miRNA21]/fM)
A
miRNA210
regenerate
Fluorescence (a.u.)
Cycle numbers
B
0week 1week 2week 3week 4week
Fluorescence (a.u.)
C
Without miRNA
miR21
miR210
miR141
let-7a
let-7c
mix
Fluorescence (a.u.)
D
Fluorescence (a. u.)
Sample ID of MCF-7
E
Fluorescence (a. u.)
Sample ID of A549
F
Fluorescence (a. u.)
Sample ID of HepG2